MATERIALS CHEMISTRY
FRONTIERS

RESEARCH ARTICLE

View Article Online
View Journal | View Issue

Cite this: *Mater. Chem. Front.*, 2018, **2**, 1165

Charge-transfer complexes based on C_{2v}-symmetric benzo[*ghi*]perylene: comparison of their dynamic and electronic properties with those of D_{6h}-symmetric coronene†

Yukihiro Yoshida, *[ab] Shunsuke Tango,[c] Kazuhide Isomura,[c] Yuto Nakamura,[c] Hideo Kishida,[c] Takashi Koretsune,[de] Masafumi Sakata,[f] Yoshiaki Nakano,[ag] Hideki Yamochi[ag] and Gunzi Saito[bh]

Received 16th March 2018,
Accepted 13th April 2018

DOI: 10.1039/c8qm00112j

rsc.li/frontiers-materials

Single crystals of three neutral charge-transfer complexes and a cation radical salt based on a C_{2v}-symmetric polycyclic aromatic hydrocarbon, benzo[*ghi*]perylene (bper), were obtained. The 1 : 1 complex with 7,7,8,8-tetracyanoquinodimethane (TCNQ) involves DA-type alternating π-columns, whereas the alternating π-columns in the 2 : 1 TCNQ complex are flanked by another bper molecule. The in-plane rotation of bper in the 1 : 1 complex was significantly suppressed compared with that of coronene in (coronene) (TCNQ), which is associated with the lower molecular symmetry of bper. Whereas the 3 : 1 TCNQ complex involves DDA-type alternating π-columns flanked by another bper molecule, bper molecules in the 3 : 1 cation radical salt with $Mo_6O_{19}^{2-}$ have a columnar structure with a [101]-like charge-ordered pattern associated with intermolecular interactions in the bay region of bper. The dimerisation of charge-rich bper molecules results in an increased energy gap at the Fermi level, and consequently, semiconducting behaviour of the salt has a larger activation energy than that of the isostructural coronene salt in the partially charged state. The lower molecular symmetry of bper also affects the degeneracy of the frontier-orbitals; the energy difference between the HOMO and the HOMO−1 of bper is significantly larger than that of coronene, which is comparable to the intermolecular transfer integrals.

Introduction

Highly symmetric polycyclic aromatic hydrocarbons (PAHs) are attractive as potential components of high-T_c superconductors owing to their degenerate frontier orbitals[1–3] and are a promising platform for artificial molecular rotors with electronic functionalities in the solid state.[3–6] Because the dynamic and electronic properties of solids largely depend on the molecular and supramolecular structures of the components, a better understanding of the structure–property relationship with a focus on the molecular symmetry of PAHs would allow the rational design of solids with desired functionalities. Over the past few years, our group has prepared a variety of charge-transfer (CT) complexes composed of the smallest D_{6h}-symmetric PAH molecule, coronene (Scheme 1) as an electron donor (D). Notably, both dicationic[7] and dianionic[8] coronene are in a thermally accessible triplet state at room temperature associated with the doubly degenerate HOMO (e_{2u}) and LUMO (e_{1g}) levels. The CT complexes range from insulating neutral complexes[9–11] to conducting cation radical salts,[12–14] and especially, some of the latter with π-stacking columns of cationic coronene show semiconducting behaviour with a high room-temperature conductivity (>1 S cm^{-1}). In addition, we found that the in-plane rotational rate of coronene molecules in CT solids can be varied by more than six orders of magnitude (1 kHz to 7 GHz at room temperature) by modifying intermolecular interactions, such as van der Waals, π–π, and hydrogen bonding interactions.

[a] *Division of Chemistry, Graduate School of Science, Kyoto University, Sakyo-ku, Kyoto 606-8502, Japan. E-mail: yoshiday@ssc.kuchem.kyoto-u.ac.jp*
[b] *Faculty of Agriculture, Meijo University, Tempaku-ku, Nagoya 468-8502, Japan*
[c] *Department of Applied Physics, Nagoya University, Chikusa-ku, Nagoya 464-8603, Japan*
[d] *Department of Physics, Tohoku University, Aoba-ku, Sendai 980-8578, Japan*
[e] *JST, PRESTO, Saitama 332-0012, Japan*
[f] *KYOKUGEN, Center for Science and Technology under Extreme Conditions, Graduate School of Engineering Science, Osaka University, Toyonaka 560-8531, Japan*
[g] *Research Center for Low Temperature and Materials Sciences, Kyoto University, Sakyo-ku, Kyoto 606-8501, Japan*
[h] *Toyota Physical and Chemical Research Institute, Nagakute 480-1192, Japan*

† Electronic supplementary information (ESI) available: Infrared spectra of TCNQ complexes (Fig. S1), crystal structure of (bper)($GaCl_4$) (Fig. S2), Kohn–Sham orbitals obtained from DFT calculations (Fig. S3). CCDC 1537813–1537817 (**1–4** and pristine bper). For ESI and crystallographic data in CIF or other electronic format see DOI: 10.1039/c8qm00112j

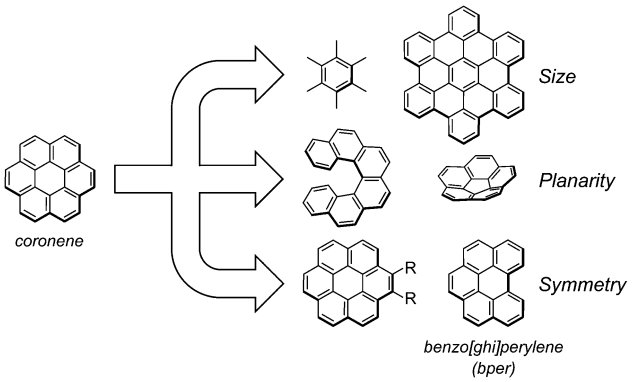

Scheme 1 Molecular structures of coronene and its analogues.

Investigation of complexes composed of coronene analogues and comparison with the corresponding coronene-based CT complexes will provide a deeper understanding of how the high symmetry of coronene affects the dynamic and electronic properties in the solid state. There are three apparent categories of coronene analogues (Scheme 1): (1) D_{6h}-symmetric polyaromatic hydrocarbons with different π-conjugated sizes (*e.g.*, hexamethylbenzene and hexa-*peri*-hexabenzocoronene),[15,16] (2) nonplanar PAHs with curved or twisted π-conjugated planes (*e.g.*, [*n*]circulene ($n \neq 6$) and [*n*]helicene),[17–21] and (3) planar PAHs with reduced symmetries (*e.g.*, 1,2-disubstituted coronene and benzo[*ghi*]-perylene (bper)).[22,23] Within the second group, we have recently realised peculiar π-electron networks in neutral CT complexes by combining corannulene (*i.e.*, [5]circulene)[24] or [6]helicene[25] as D with planar 7,7,8,8-tetracyanoquinodimethane (TCNQ) analogues as electron acceptors (A's). In search of CT complexes using PAHs in the third group, we focus on C_{2v}-symmetric bper, which is regarded as a coronene analogue that has lost a benzene ring; unlike 1,2-disubstituted coronene, bper has no bulky substituents and has the higher electron donating ability ($E^1_{1/2}$(D) = 1.01 V *vs.* saturated calomel electrode (SCE)) than that of coronene (1.23 V).[26] In the solid state, bulky substituents inevitably inhibit intermolecular π–π interactions, which are indispensable for the formation of a π-conduction network, and the appropriate electron-donating ability allows the formation of stable CT complexes under aerobic conditions. Herein, we report the synthesis and the structural, optical, and transport properties of neutral CT complexes with TCNQ having different compositions (**1–3**) and a cation radical salt with a hexamolybdate ($Mo_6O_{19}^{2-}$) cluster unit (**4**), with the support of theoretical calculations. Crystallographic data were also used to assess the thermal fluctuations, which are indicative of in-plane molecular rotations, of bper molecules in the solid state.

Results

(bper)(TCNQ) (**1**) and (bper)$_3$(TCNQ) (**3**) were prepared by the solvent evaporation method, whereas (bper)$_2$(TCNQ) (**2**) was obtained preferentially by the co-sublimation method. (bper)$_3$Mo$_6$O$_{19}$ (**4**) was obtained by the electrochemical oxidation of bper in the presence of an electrolyte, $(Bu_4N)_2Mo_6O_{19}$ (see Experimental and computational for details). The crystal structures of **1–4** were determined at 100 K (Table 1).

Charge transfer

Regardless of composition, complexes **1–3** exhibit a CT absorption band at around $h\nu_{CT} = 12 \times 10^3$ cm^{-1} in addition to the intramolecular transition bands of the component molecules above 20×10^3 cm^{-1} (Fig. 1a). These $h\nu_{CT}$ values are lower than those of coronene–TCNQ complexes (14×10^3 cm^{-1})[9] because

Table 1 Crystallographic data of **1–4**

	(bper)(TCNQ) (**1**)	(bper)$_2$(TCNQ) (**2**)	(bper)$_3$(TCNQ) (**3**)	(bper)$_3$Mo$_6$O$_{19}$ (**4**)
Formula	$C_{34}H_{16}N_4$	$C_{56}H_{28}N_4$	$C_{78}H_{40}N_4$	$C_{66}H_{36}Mo_6O_{19}$
Formula weight	480.53	756.87	1033.20	1708.64
Crystal system	Orthorhombic	Triclinic	Triclinic	Triclinic
Space group	$P2_12_12_1$	$P\bar{1}$	$P\bar{1}$	$P\bar{1}$
Crystal size (mm^3)	0.49 × 0.09 × 0.06	0.20 × 0.08 × 0.07	0.50 × 0.07 × 0.04	0.56 × 0.08 × 0.04
a (Å)	7.1719(4)	7.1246(8)	10.0725(14)	9.8455(9)
b (Å)	10.8284(5)	12.3495(14)	10.8786(15)	11.0998(10)
c (Å)	29.7864(15)	21.257(3)	12.9332(18)	12.8243(11)
α (deg)	90	78.598(2)	113.110(2)	86.101(1)
β (deg)	90	80.637(2)	105.578(2)	67.763(1)
γ (deg)	90	80.207(2)	90.301(2)	89.093(1)
V (Å^3)	2313.2(2)	1790.4(4)	1245.7(3)	1294.2(2)
Z	4	2	1	1
Temperature (K)	100	100	100	100
d_{calc} (g cm^{-3})	1.380	1.404	1.377	2.192
μ(Mo Kα) (mm^{-1})	0.083	0.083	0.080	1.499
Reflns used	4716	6295	5057	5122
Refined params	343	541	469	511
R_1 (for $I > 2\sigma(I)$)[a]	0.0386	0.0783	0.0490	0.0204
wR_2 (for all data)[b]	0.0799	0.1755	0.1189	0.0515
GOF on F^2	1.030	1.003	1.003	1.026
CCDC	1537813	1537814	1537815	1537816

[a] $R_1 = \sum(|F_o| - |F_c|)/\sum|F_o|$. [b] $wR_2 = [\sum w(F_o^2 - F_c^2)^2/\sum w(F_o^2)^2]^{0.5}$.

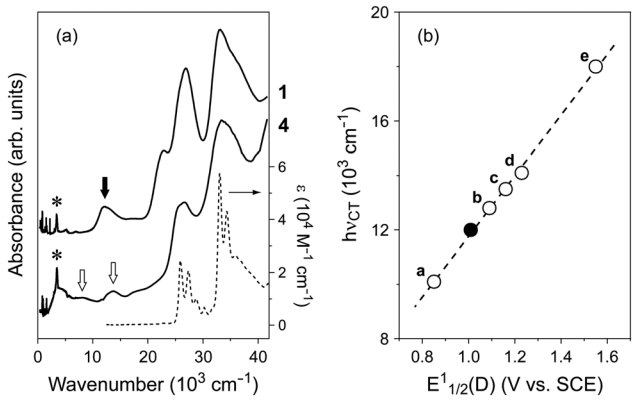

Fig. 1 (a) Absorption spectra of **1** and **4** measured on KBr pellets (solid lines) together with pristine bper in 10^{-5} M chloroform solution (dotted line). Closed and open arrows indicate the bands originating from an intermolecular charge transfer transition between neutral bper and TCNQ and an intramolecular transition of monocationic bper, respectively. Asterisks indicate the band originating from the O–H stretching mode of water molecules absorbed in the KBr powder. (b) Plot of CT energy ($h\nu_{CT}$) against the first redox potential of PAH molecules ($E^1_{1/2}$(D)) in TCNQ complexes (closed circle: **1–3**, a: (perylene)(TCNQ),[29] b: (anthracene)(TCNQ),[30] c: (pyrene)(TCNQ),[31] d: (coronene)(TCNQ),[9,32] e: (triphenylene)$_2$(TCNQ)(toluene)[33]).

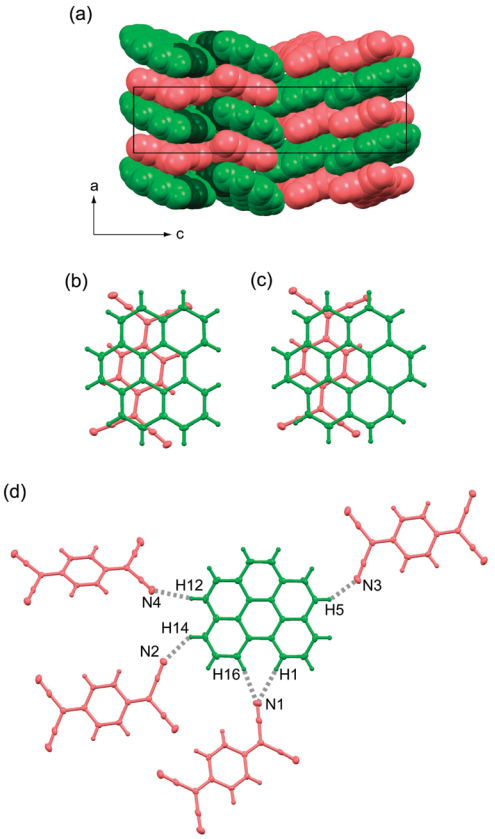

Fig. 2 (a) Molecular packing of **1** viewed along the *b* axis in a space-fill representation. Bper and TCNQ molecules appear in green and red, respectively, where carbon and hydrogen atoms in the bay region are darkened. Overlap patterns of adjacent PAH and TCNQ molecules within a column viewed perpendicularly to the molecular plane of PAH in (b) **1** and (c) (coronene)(TCNQ).[9,32] (d) C–H···N hydrogen bonds around bper molecule in **1** along the side-by-side direction.

the electron-donating ability of bper is stronger than that of coronene.[27,28] As shown in Fig. 1b, complexes **1–3** lie on the straight line obtained by applying a least-squares method to the plots of $h\nu_{CT}$ against $E^1_{1/2}$(D) for the TCNQ complexes of typical PAH molecules (perylene,[29] anthracene,[30] pyrene,[31] coronene,[9,32] and triphenylene[33]). Bond length analysis based on crystallographic data[34] estimates the charge of the TCNQ molecules to be −0.14(3) for **1**, −0.23(9) for **2**, and −0.17(4) for **3**, which are the same within experimental error. Infrared spectra support the neutral nature (Fig. S1 in ESI†).

Salt **4** exhibits the distinct bands at 8.1 and 13.7 × 10^3 cm^{-1}, which are reminiscent of the absorption spectra of the bper monocation isolated in matrices.[35–37] This spectral feature is firm evidence that this salt is the first example of a solid composed of cationic bper. The salt also exhibits a low-lying band with a maximum at approximately 4 × 10^3 cm^{-1}, which arises from the intermolecular transition between neutral and monocationic bper molecules,[38] as expected from the X-ray diffraction measurements (*vide infra*).

(bper)(TCNQ) (1). Complex **1** crystallises in a non-centrosymmetric orthorhombic lattice with space group $P2_12_12_1$, and each bper and TCNQ molecule is crystallographically independent. The complex involves DA-type alternating π-stacking columns (Fig. 2a) with a ring-over-bond pattern (Fig. 2b) along the *a* axis, as in (coronene)(TCNQ) (Fig. 2c).[9,32] Within the column, bper molecules are aligned in the same direction because each unit cell along the *a* direction contains only one bper molecule. Adjacent bper and TCNQ molecules are arranged in a nonparallel fashion, and the interplanar distance, which is defined as half the distance between bper molecules across a TCNQ molecule, was estimated to be 3.27 Å. It should be noted that the dihedral angle (θ) between bper and TCNQ molecules within the column (3.36°) is apparently larger than that in (coronene)(TCNQ) (2.40°), but the interplanar distance is comparable to that in (coronene)(TCNQ) (3.26 Å).[9] Along the side-by-side direction, each bper molecule is connected to four adjacent TCNQ molecules (Fig. 2d) through C–H···N hydrogen bonds (H1···N1: 2.72 Å, H16···N1: 2.63 Å, H14···N2: 2.75 Å, H12···N4: 2.61 Å, H5···N3: 2.69 Å *vs.* sum of van der Waals radii: 2.75 Å[39]).

(bper)$_2$(TCNQ) (2). Complex **2** has lower crystal symmetry (centrosymmetric triclinic $P\bar{1}$) than **1**, and the asymmetric unit contains two bper molecules (denoted as **bper-2A** and **bper-2B**) and one TCNQ molecule. In the crystal, the **bper-2A** molecules construct a DA-type alternating π-stacking column with TCNQ along the *a* axis, whereas **bper-2B**, which has a tilt angle with respect to **bper-2A** of 84.3°, separates the neighbouring columns approximately along the [1 −1 0] direction (Fig. 3a). A coronene–TCNQ CT complex with a 2 : 1 ratio has not been obtained at present, but (perylene)$_2$TCNQ with the same packing motif was recently prepared by Vermeulen *et al.*[40] Within the column, adjacent **bper-2A** and TCNQ molecules, whose molecular planes are slightly inclined to each other (θ = 0.79°), display a ring-over-bond overlap pattern (Fig. 3b). Along the side-by-side direction, each **bper-2A** molecule forms short interatomic contacts with

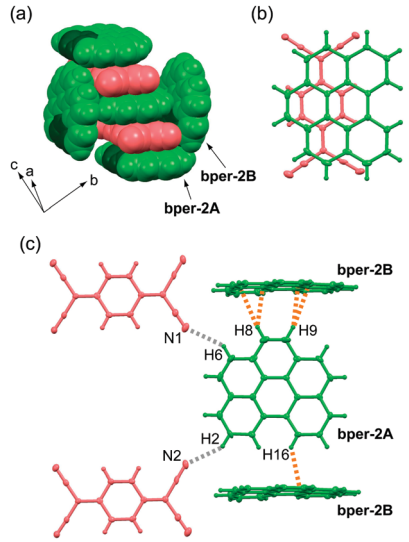

Fig. 3 (a) Molecular arrangement of **2** in a space-fill representation. Bper and TCNQ molecules appear in green and red, respectively, where carbon and hydrogen atoms in the bay region are darkened. (b) Overlap pattern of adjacent **bper-2A** and TCNQ molecules within a column viewed perpendicularly to the molecular plane of **bper-2A** in **2**. (c) Short interatomic contacts around one **bper-2A** molecule with surrounding **bper-2B** and TCNQ molecules in **2**. The gray and orange dotted lines show C–H···N and C–H···C (or C–H···π) hydrogen bonds, respectively.

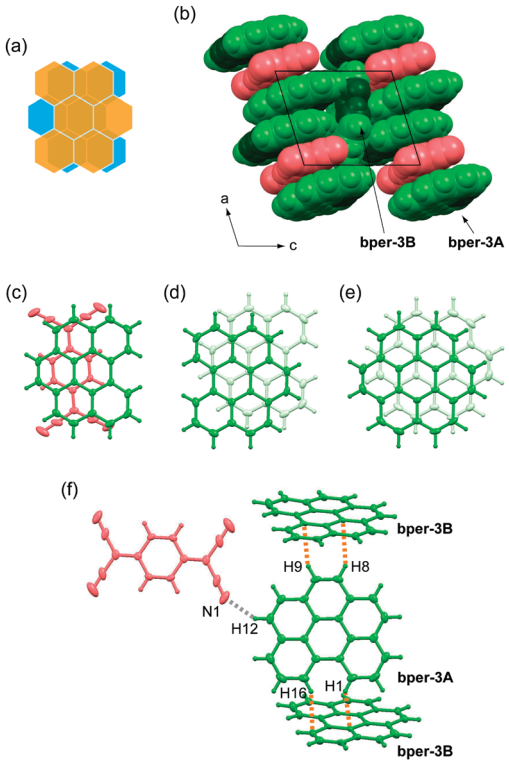

Fig. 4 (a) Schematic representation of the disorder of **bper-3B** molecule in **3**. (b) Molecular packing of **3** viewed along the *b* axis in a space-fill representation. Bper and TCNQ molecules appear in green and red, respectively, where carbon and hydrogen atoms in the bay region are darkened. (c) Overlap pattern of adjacent **bper-3A** and TCNQ molecules within a column viewed perpendicularly to the molecular plane of **bper-3A** in **3**. Overlap patterns of adjacent PAH molecules within a column viewed perpendicularly to the molecular plane of PAH in (d) **3** and (e) (coronene)$_3$(TCNQ).[9,32] (f) Short interatomic contacts around one **bper-3A** molecule with surrounding **bper-3B** and TCNQ molecules in **3**. The gray and orange dotted lines show C–H···N and C–H···C (or C–H···π) hydrogen bonds, respectively.

two **bper-2B** molecules through C–H···π hydrogen bonds (≈2.9 Å;[39,41,42] the observed C–H···C distances are 2.65–2.89 Å) and two TCNQ molecules through C–H···N hydrogen bonds (H2···N2: 2.66 Å, H6···N1: 2.73 Å), as shown in Fig. 3c.

(bper)$_3$(TCNQ) (3). Complex **3** also belongs to the centrosymmetric triclinic system with space group $P\bar{1}$ and is isostructural with (coronene)$_3$(TCNQ).[9] The asymmetric unit includes one and a half bper molecules (denoted as **bper-3A** and **bper-3B**, respectively) and half a TCNQ molecule; **bper-3B** is disordered over two orientations, which are related by an inversion center, with equivalent occupancy factors of 0.5 (Fig. 4a). As shown in Fig. 4b, the complex involves DDA-type alternating π-stacking columns with a [**bper-3A**···**bper-3A**···TCNQ] repeating unit along the *a* axis. As in the case of **2**, the column is flanked by another bper molecule (**bper-3B**) with a tilt angle of 69.8° with respect to **bper-3A**. The ring-over-bond-type overlap pattern between **bper-3A** and TCNQ (Fig. 4c) is reminiscent of those in **1** and **2**, and the molecular planes are slightly inclined to each other (θ = 0.97°). Adjacent **bper-3A** molecules within the column are oriented in the opposite direction with a ring-over-atom overlap pattern on an inversion center (Fig. 4d), in contrast to the ring-over-bond overlap pattern in pristine bper crystal[43,44] with a "sandwich herringbone structure"[45] and the same interplanar distance (3.37 Å). A shift along the in-plane direction (2.67 Å) is significantly larger than that in (coronene)$_3$(TCNQ) (1.50 Å; Fig. 4e) with a longer interplanar distance (3.43 Å).[9] As shown in Fig. 4f, each **bper-3A** molecule is connected to two **bper-3B** molecules through C–H···π hydrogen bonds (the observed C–H···C distances are 2.70–2.89 Å) and one TCNQ molecule through a C–H···N hydrogen bond (H12···N1: 2.70 Å).

(bper)$_3$Mo$_6$O$_{19}$ (4). Salt **4** is the first cation radical solid based on bper, and the triclinic lattice (space group $P\bar{1}$) is isostructural with (coronene)$_3$Mo$_6$O$_{19}$.[13] One and a half bper molecules (denoted as **bper-4A** and **bper-4B**, respectively) and half a $Mo_6O_{19}^{2-}$ cluster unit are crystallographically independent; namely, **bper-4B** and $Mo_6O_{19}^{2-}$ are located on an inversion center. Similar to **bper-3B** in **3**, **bper-4B** is disordered over two orientations with equivalent occupancy factors of 0.5 (Fig. 5a). Notably, the salt forms a segregated π-stacking column with a [**bper-4A**···**bper-4A**···**bper-4B**] repeating unit along the *a* axis (Fig. 5b). Such a cationic column has been reported for several PAH molecules.[46–50] Within the column, adjacent **bper-4A** molecules oriented in the opposite direction display a ring-over-bond overlap pattern (Fig. 5c) with an interplanar distance of 3.14 Å, which is similar to that in isostructural (coronene)$_3$Mo$_6$O$_{19}$ (3.16 Å; ring-over-atom).[13] This distance is significantly shorter than those in natural graphite (3.35 Å; ring-over-atom),[51] pristine bper crystal (3.36 Å; ring-over-bond),[43,44] and **3** (3.37 Å; ring-over-atom), possibly due to stabilisation of the partially occupied HOMO of each **bper-4A**. In contrast, adjacent **bper-4A** and **bper-4B** molecules are nonparallel with a dihedral angle of 3.9°; one of the

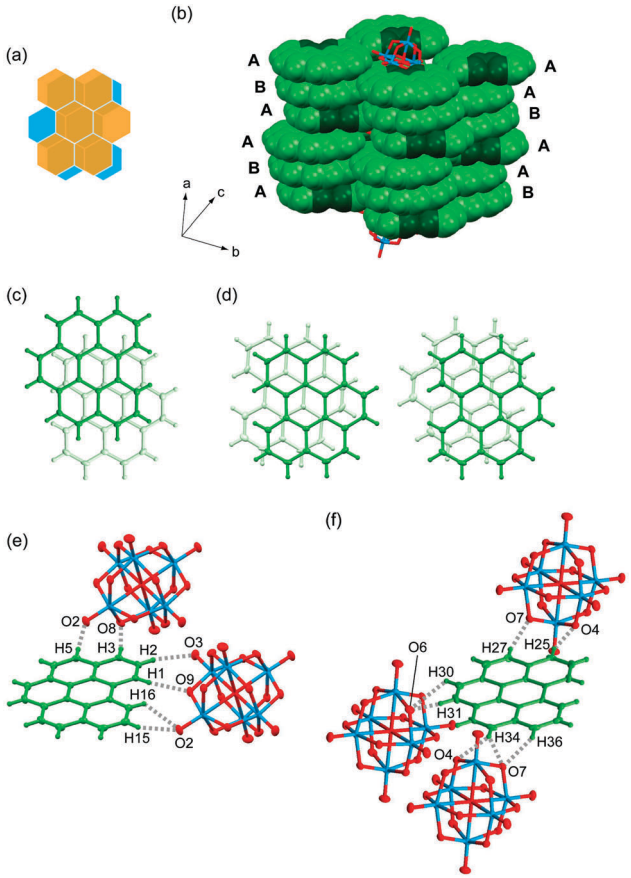

Fig. 5 (a) Schematic representation of the disorder of **bper-4B** molecule in **4**. (b) Columnar structure of bper molecules in **4** in a space-fill representation, where carbon and hydrogen atoms in the bay region are darkened. **A** and **B** indicate the **bper-4A** and **bper-4B** molecules, respectively. Overlap patterns of (c) adjacent **bper-4A** molecules and (d) adjacent **bper-4A** and **bper-4B** molecules with two possible orientations within a column viewed perpendicularly to the molecular plane of **bper-4A** in **4**. C–H···O hydrogen bonds around (e) **bper-4A** and (f) one orientation of disordered **bper-4B** in **4** along the side-by-side direction.

disordered **bper-4B** molecules is oriented in the same direction as **bper-4A**, whereas the other is oriented in the opposite direction (Fig. 5d). Notably, the interplanar distance, which is defined as half the distance between two **bper-4A** molecules separated by a **bper-4B** molecule, was estimated to be 3.28 Å, which is significantly longer than that in $(coronene)_3Mo_6O_{19}$ (3.19 Å).[13]

Each **bper-4A** molecule interacts with two adjacent $Mo_6O_{19}^{2-}$ cluster units along the side-by-side direction through C–H···O hydrogen bonds (H15···O2: 2.67 Å, H16···O2: 2.58 Å, H1···O9: 2.49 Å, H2···O3: 2.50 Å, H3···O8: 2.43 Å, H5···O2: 2.41 Å *vs.* sum of van der Waals radii: 2.72 Å;[39] Fig. 5e). Notably, hydrogen atoms in the bay region of **bper-4A** are essential for the formation of quadruple hydrogen bonds with an adjacent $Mo_6O_{19}^{2-}$ cluster unit. Fig. 5f shows the short interatomic contacts between one orientation of disordered **bper-4B** and $Mo_6O_{19}^{2-}$ along the side-by-side direction. Each **bper-4B** molecule forms C–H···O hydrogen bonds with three adjacent $Mo_6O_{19}^{2-}$ cluster units through double or triple C–H···O hydrogen bonds (H36···O7: 2.68 Å, H34···O7: 2.52 Å, H34···O4: 2.50 Å, H31···O6: 2.63 Å, H30···O6: 2.64 Å, H27···O7: 2.67 Å, H25···O4: 2.37 Å). Unlike the case of **bper-4A**, hydrogen atoms in the bay region of **bper-4B** make no contribution to hydrogen bond formation.

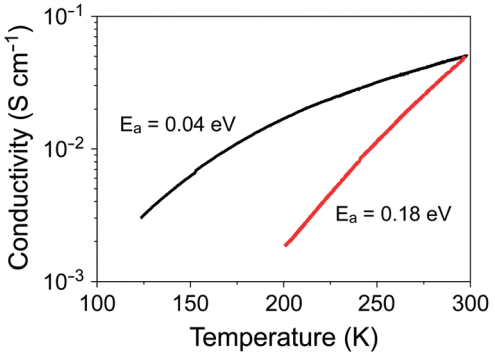

Fig. 6 Temperature dependence of the electrical conductivity of a single crystal of **4** (red line) and $(coronene)_3Mo_6O_{19}$ (black line).[13]

Resistivity measurements were performed to investigate the effect of molecular symmetry on the electronic properties. Fig. 6 shows the temperature dependence of the electrical conductivity (σ) of a single crystal of **4**, which has a room-temperature value of 5×10^{-2} S cm^{-1} similar to that of $(coronene)_3Mo_6O_{19}$.[13] However, a marked difference between the two salts was observed upon cooling; namely, the σ value of **4** decreases steeply with decreasing temperature. The activation energy of **4** was estimated to be 0.18 eV, which is more than four times that of $(coronene)_3Mo_6O_{19}$ (0.04 eV).

Discussion

Effect of molecular structure on dynamic properties

Solid-state NMR spectroscopy has become a definitive experimental technique for investigating the dynamic properties of molecular rotators in the solid state.[3,5,6] Despite this demonstrated utility, the deuteration of bper is unavailable at the present stage. Another way to assess the dynamic behaviour of molecules is to examine the magnitude and anisotropy of thermal fluctuations based on crystallographic data. Indeed, coronene molecules, whose fast in-plane 6-fold flipping motion was confirmed by the ^{2}H NMR spectra of the deuterated complexes, exhibit large thermal fluctuations along the in-plane direction.[9,11] As shown in Fig. 7a, the in-plane thermal fluctuations of bper molecules in **1** at room temperature are less pronounced than those of (coronene)(TCNQ) (Fig. 7b);[9] the average mean-square displacement of component carbon atoms, $\langle\mu^2\rangle$, was estimated to be 0.062 Å^2 for bper in **1** and 0.145 Å^2 for coronene in (coronene)(TCNQ) at 298 K. Thus, the in-plane rotation of bper is significantly suppressed by the loss of a benzene ring, even though **1** has a larger θ value than (coronene)(TCNQ).

To shed light on this phenomenon, we investigate the temperature dependence of the relative $\langle\mu^2\rangle$ value with respect of that of TCNQ in **1**, as previously performed for (coronene)(TCNQ).[9] As shown in Fig. 7c, the coronene complex shows a rapid increase in $\langle\mu^2\rangle_{PAH}/\langle\mu^2\rangle_{TCNQ}$ at around 200 K, above which the angle between

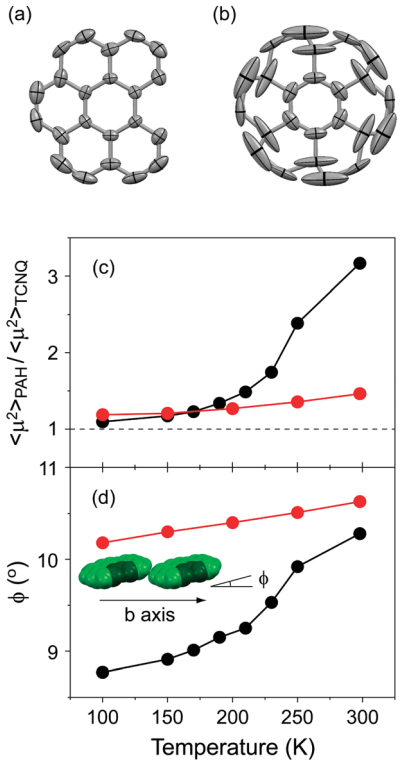

Fig. 7 Thermal fluctuations of (a) bper in **1** and (b) coronene in (coronene)(TCNQ)[9] at 298 K viewed perpendicular to the molecular plane. Hydrogen atoms are omitted for clarity, and the 50% probability thermal ellipsoids are shown. Temperature dependence of (c) relative $\langle\mu^2\rangle$ values of PAH (bper or coronene) with respect of that of TCNQ ($\langle\mu^2\rangle_{PAH}/\langle\mu^2\rangle_{TCNQ}$) and (d) angles between the PAH plane and the crystallographic axis along the side-by-side direction (ϕ) in each CT solid (red circles: **1**, black circles: (coronene)(TCNQ)).[9] The inset shows the arrangement of bper molecules in **1** along the *b* axis.

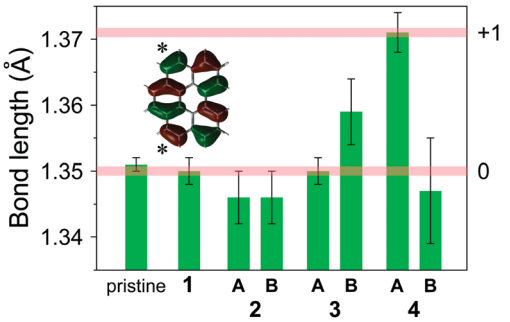

Fig. 8 Lengths of the bonds marked by an asterisk in the inset for pristine bper crystal and **1–4**. The pale red horizontal lines mark the estimated values for monocationic (upper) and neutral (lower) bper molecules. The inset shows the HOMO distribution of a bper molecule calculated by DFT methods at the RB3LYP/6-31+G(d,p) level of theory.

the coronene plane and the crystallographic *a* axis (ϕ; Fig. 7d) also steeply increases to accelerate molecular rotation. In contrast, for **1**, neither parameter shows such an anomaly in the measured temperature region (100–298 K). The origin of the effect on the dynamic properties of these complexes is not determined from the crystallographic data. However, the difference in the relationship between $\langle\mu^2\rangle_{PAH}/\langle\mu^2\rangle_{TCNQ}$ and ϕ provides clear evidence for the importance of intermolecular interactions in determining the dynamic properties. Considering that the decreased axial symmetry of a rotator leads to an increase in the rotational barrier as well as a decrease in the number of energy maxima and minima,[6] it is apparent that the lower molecular symmetry of bper is a dominant factor in suppressing the displacement that accompanies molecular rotation.

Effect of molecular structure on charge state

The bonds marked by an asterisk in the inset of Fig. 8, which have bonding character in the HOMO level, were found to have similar lengths in pristine bper crystal and neutral CT complexes **1–3** (except for **bper-3B**), whereas those in **bper-4A** are longer than them by *ca.* 0.02 Å (Fig. 8). Considering that the bond lengths in **bper-4B** are comparable to those observed in the neutral species, **bper-4B** is in a nearly neutral state and **bper-4A** must be in a nearly monocationic state to construct a [101]-like charge-ordered column.[52,53] Thus, the low-lying absorption band at around 4×10^3 cm^{-1} shown in Fig. 1a can be assigned to electron transfer between cationic **bper-4A** and neutral **bper-4B**. Although the reason that the bonds in **bper-3B** are longer than expected is unclear, density functional theory (DFT) calculations at the B3LYP/6-31+G(d,p) level of theory (Fig. S3 in ESI†) show that the bonds in the bper monocation are elongated by 0.017 Å relative to those in neutral bper, which quantitatively supports the experimental results. First principles calculations within DFT based on the crystallographic data estimate the charges of **bper-4A** and **bper-4B** to be +0.82 and +0.37, respectively.[54]

Apparently, compared with (coronene)$_3$Mo$_6$O$_{19}$, the removal of a benzene ring from a coronene molecule results in looser molecular packing in **4**, as manifested by the orientational disorder of **bper-4B**. This disorder is an indication that the Coulombic interactions of **bper-4B** with $Mo_6O_{19}^{2-}$ through hydrogen bonds are weaker than those for **bper-4A**, which forms quadruple hydrogen bonds with $Mo_6O_{19}^{2-}$ in the bay region. It is possible that the difference in intermolecular interactions plays a key role in the emergence of charge disproportionation, namely, charge-rich **bper-4A** and charge-poor **bper-4B**.

To elucidate the relationship between molecular symmetry and the electronic properties, we focus on the interplanar distances within the column as described above. It appears that those in **4** and (coronene)$_3$Mo$_6$O$_{19}$[13] bear some similarities together with striking differences; namely, the distance between adjacent monocationic **bper-4A** molecules is similar to that in (coronene)$_3$Mo$_6$O$_{19}$ to stabilise the partially occupied HOMO of **bper-4A** (3.14 Å in **4** *vs.* 3.16 Å in (coronene)$_3$Mo$_6$O$_{19}$), whereas the distance between **bper-4A** and **bper-4B** (3.28 Å) is significantly longer than that in (coronene)$_3$Mo$_6$O$_{19}$ (3.19 Å) possibly due to the neutral character of **bper-4B**. The intermolecular transfer integrals for **4** at 100 K calculated by the first principles method within DFT (277 meV between **bper-4A** and **bper-4A** and 100–159 meV between **bper-4A** and **bper-4B**) have a remarkable alternation relative to the case in (coronene)$_3$Mo$_6$O$_{19}$ (257 and 208–219 meV, respectively) owing to the increased distance

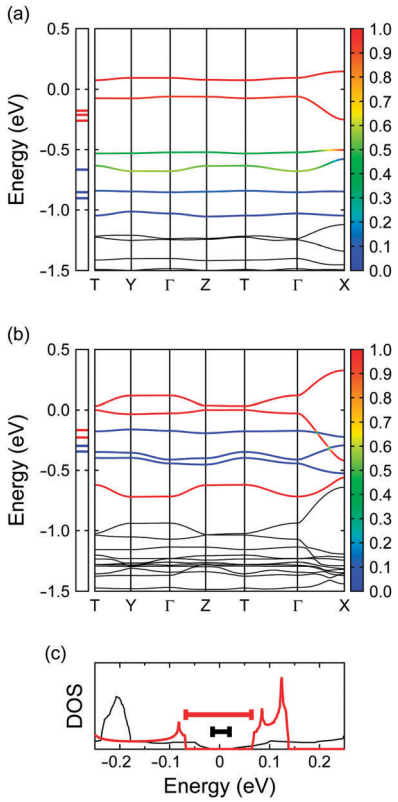

Fig. 9 DFT energy band structures of (a) **4** and (b) $(coronene)_3Mo_6O_{19}$,[13] calculated by first principles methods using the crystallographic data at 100 K, where *T* is (0, 1/2, 1/2) and the energy is given relative to the Fermi energy. The coloration of the six highest branches represents the fraction of HOMO (red) and HOMO−1 (blue) components. Red and blue horizontal ticks in the left box indicate the energy levels of the HOMO and the HOMO−1, respectively. (c) Density of states (DOS) of **4** (red) and $(coronene)_3Mo_6O_{19}$ (black)[13] near the Fermi energy, where the thick red and black bars indicate the energy gaps.

between **bper-4A** and **bper-4B**. As shown in Fig. 9a and b, this alternation inevitably gives rise to decreased band dispersion accompanied by an increased energy gap at the Fermi level (124 meV) compared with that in $(coronene)_3Mo_6O_{19}$ (32 meV). It appears that the increased energy gap is responsible for the semiconducting behaviour with a larger activation energy, as mentioned above; namely, these salts can be regarded as band insulators. The exceptionally small activation energy of $(coronene)_3Mo_6O_{19}$ largely depends on the highly symmetric molecular structure of coronene.

Effect of molecular structure on orbital degeneracy

One of the most striking effects of molecular symmetry on π-electronic systems, which has an impact on electronic properties, is orbital degeneracy. As reported previously, the energy difference between the HOMO and the HOMO−1 of coronene (Jahn–Teller splitting) in $(coronene)_3Mo_6O_{19}$ is very small (*ca.* 0.12 eV; Fig. 9a and c) and comparable to the intermolecular transfer integrals.[13] It is noteworthy that this value is similar to that in C_{60} anions (0.06–0.12 eV).[55] In contrast, the energy difference in **4** (*ca.* 0.59 eV; Fig. 9b and c) is about five times greater than that in $(coronene)_3Mo_6O_{19}$ due to the decreased molecular symmetry. This marked difference distinctly indicates that the HOMO and HOMO−1 energy levels in $(coronene)_3Mo_6O_{19}$ are almost degenerate despite the reduced symmetry of the crystal field (space group $P\bar{1}$). If cationic coronene molecules could be stacked uniformly in solids, the density of states (DOS) of the HOMO/HOMO−1 band would likely be enhanced because of the orbital degeneracy. Subsequent adjustment of the Fermi level to the high DOS region may produce a new class of organic superconductors within the Bardeen–Cooper–Schrieffer (BCS) framework through electron–phonon coupling.[1–3] Studies along this line are now in progress.

Conclusions

In the present study, the influence of the molecular symmetry of planar PAH molecules on dynamic and electronic properties was investigated by comparing compounds of C_{2v}-symmetric bper with corresponding compounds of D_{6h}-symmetric coronene. It was found that the removal of a benzene ring from the coronene molecule significantly suppresses molecular rotation along the in-plane direction in the solid state. In addition, the lower molecular symmetry of bper leads to charge ordering associated with the formation of significant hydrogen bonds with counter anions in the bay region, which is responsible for enhanced alternation of interplanar distances and transfer integrals within the column. These features inevitably result in an increased energy gap at the Fermi level, which corresponds to semiconducting behaviour with a large activation energy. Isostructural cation radical salts composed of PAH molecules with different symmetries enable investigations of the effect of molecular symmetry on the degeneracy of frontier orbitals in the solid state; namely, a comparison with the present bper-based cation radical salt revealed that the doubly degenerate HOMO of coronene molecules is maintained, even though the cation radical salt has a low-symmetry crystal field.

Experimental and computational

Materials and methods

Dichloromethane and pentane were used as received (Wako Chemicals), whereas methanol, chloroform, and acetone were distilled prior to use. Bper was purchased from Aldrich and used without any further purification. TCNQ was purified by sublimation prior to use, and $(Bu_4N)_2Mo_6O_{19}$ was synthesized and recrystallised from acetone according to the literature procedure.[56]

Synthesis of (bper)(TCNQ) (1). Equimolar amounts of bper and TCNQ (0.017 mmol) was dissolved in 50 mL of dichloromethane/pentane (1 : 1). Natural evaporation of the solution at room temperature yielded *ca.* 3 mg (0.006 mmol) of black needle-shaped crystals of **1** (yield: 37%).

Synthesis of $(bper)_2(TCNQ)$ (2). Equimolar amounts of bper and TCNQ (0.020 mmol) were ground together in an agate mortar and transferred into a 12 mm-diameter borosilicate glass tube.

After sealing under vacuum (5.8×10^{-5} mbar), the 13 cm-long tube was placed in a two-zone furnace with a temperature gradient from 220 °C (sample side) to 150 °C (opposite side). After heating for 2 days, black thick plate crystals of **2** were grown on the center area in the tube (yield: *ca.* 50%).

Synthesis of (bper)$_3$(TCNQ) (3). Equimolar amounts of bper and TCNQ (0.050 mmol) were added to 20 mL of dichloromethane/pentane (1 : 1). After stirring at room temperature, the suspension was filtered to remove any traces of undissolved TCNQ. The filtrate was removed by natural evaporation at room temperature to yield *ca.* 10 mg (0.010 mmol) of black needle-shaped crystals of **3** (yield: 58%).

Synthesis of (bper)$_3$Mo$_6$O$_{19}$ (4). Bper (0.016 mmol) and $(Bu_4N)_2Mo_6O_{19}$ (0.022 mmol) were added to the anodic and cathodic compartments, respectively, in an H-shaped cell. After the cell was vacuum-dried, 18 mL of dichloromethane and a few drops of methanol were added to the cell. A constant current (1.0 μA) was passed between the two platinum electrodes. Black needle-shaped crystals of **4** were grown on the anodic electrode over a period of 2 weeks at 15 °C (yield: *ca.* 50%).

Spectroscopy. UV-Vis-NIR absorption spectra were measured on KBr pellets ($3.8–42 \times 10^3$ cm^{-1}) or in a chloroform solution ($12–50 \times 10^3$ cm^{-1}) using a Shimadzu UV-3100 spectrophotometer.

X-Ray structural analysis. Single-crystal X-ray diffraction experiments were performed on a CCD-type diffractometer (Bruker SMART APEX II) with graphite-monochromated Mo Kα radiation (λ = 0.71073 Å) at 100 K. A single crystal was mounted on a glass capillary and cooled by a stream of cooled nitrogen gas. The crystal structures were solved by a direct method using the SIR2004 program[57] and were refined by a full-matrix least-squares method on F^2 using the SHELXL program.[58] All non-hydrogen atoms were anisotropically refined. The positional parameters of the hydrogen atoms were calculated under the assumption of fixed C–H bond lengths of 0.93 Å with sp^2 configuration of the parent atoms.

Resistivity measurements. Electrical resistivity of **4** was measured using a conventional four-probe method using a Keithley 2000 multimeter. Gold wires (ϕ = 10 μm) were attached to a single crystal with carbon paint (DOTITE XC-12). A DC current of less than 10 μA was applied along the stacking direction (crystal long axis).

Theoretical calculations (single molecule). DFT calculations with the B3LYP functional[59] were carried out with the 6-31+G(d,p) basis set.[60,61] To ensure the reliability of the frequencies, both ''Opt = Tight'' and ''Int = Ultrafine'' were specified. The stabilities of the wave functions were confirmed by specifying the ''Stable = Opt'' keyword in the present DFT calculations. All the computations were performed using the Gaussian 09 program package,[62] in which the bper molecule lies on the *yz* plane.

Theoretical calculations (band). Using the experimental structure, we performed the electronic structure calculations within the generalised gradient approximation[63] in the framework of the density functional theory as implemented in the quantum-ESPRESSO code.[64] Ultrasoft pseudopotentials[65] and the plane-wave basis set with cutoff energies of 30 Ry for wave functions and 150 Ry for charge densities were used. To obtain the transfer integrals, we constructed six maximally-localized Wannier orbitals[66,67] from the six bands at the top of the valence band, which correspond to HOMO and HOMO−1 of each bper molecule. Charge disproportionation was discussed by diagonalising this six-band model.

Conflicts of interest

There are no conflicts to declare.

Acknowledgements

This work was supported by the Japan Society for the Promotion of Science (JSPS) KAKENHI Grant Numbers JP25288041 and JP16H04139 (YY), JP16H00924 (TK), JP15K17901 and JP17H05153 (Y. Nakano), JP26288035 (HY), JP26110512 and JP16H00964 (HK), and JP23225005 (GS) and by JST PRESTO (TK). Theoretical calculations were partly performed at Research Center for Computational Science, Okazaki, Japan, and the SuperComputer System, Institute for Chemical Research, Kyoto University, Japan.

Notes and references

1 O. Gunnarsson, *Rev. Mod. Phys.*, 1997, **69**, 575.
2 M. J. Rosseinsky, *Chem. Mater.*, 1998, **10**, 2665.
3 Y. Yoshida, K. Isomura, Y. Kumagai, M. Maesato, H. Kishida, M. Mizuno and G. Saito, *J. Phys.: Condens. Matter*, 2016, **28**, 304001.
4 R. K. Boyd, C. A. Fyfe and D. A. Wright, *J. Phys. Chem. Solids*, 1974, **35**, 1355.
5 T. Akutagawa, *Mater. Chem. Front.*, 2018, DOI: 10.1039/C7QM00603A.
6 C. S. Vogelsberg and M. A. Garcia-Garibay, *Chem. Soc. Rev.*, 2012, **41**, 1892.
7 P. J. Krusic and E. Wasserman, *J. Am. Chem. Soc.*, 1991, **113**, 2322.
8 M. Glasbeek, J. D. W. van Voorst and G. J. Holjtink, *J. Chem. Phys.*, 1966, **45**, 1852.
9 Y. Yoshida, Y. Shimizu, T. Yajima, G. Maruta, S. Takeda, Y. Nakano, T. Hiramatsu, H. Kageyama, H. Yamochi and G. Saito, *Chem. – Eur. J.*, 2013, **19**, 12313.
10 Y. Yoshida, Y. Kumagai, M. Mizuno and G. Saito, *Cryst. Growth Des.*, 2015, **15**, 1389.
11 Y. Yoshida, Y. Kumagai, M. Mizuno, K. Isomura, Y. Nakamura, H. Kishida and G. Saito, *Cryst. Growth Des.*, 2015, **15**, 5513.
12 Y. Yoshida, M. Maesato, Y. Kumagai, M. Mizuno, K. Isomura, H. Kishida, M. Izumi, Y. Kubozono, A. Otsuka, H. Yamochi, G. Saito, K. Kirakci, S. Cordier and C. Perrin, *Eur. J. Inorg. Chem.*, 2014, 3871.
13 Y. Yoshida, K. Isomura, H. Kishida, Y. Kumagai, M. Mizuno, M. Sakata, T. Koretsune, Y. Nakano, H. Yamochi, M. Maesato and G. Saito, *Chem. – Eur. J.*, 2016, **22**, 6023.
14 Y. Yoshida, K. Isomura, M. Maesato, T. Koretsune, Y. Nakano, H. Yamochi, H. Kishida and G. Saito, *Cryst. Growth Des.*, 2016, **16**, 5994.

15 R. Foster, *Organic Charge-Transfer Complexes*, Academic Press, London, 1969.
16 M. D. Watson, A. Fechtenkötter and K. Müllen, *Chem. Rev.*, 2001, **101**, 1267.
17 *Fragments of Fullerenes and Carbon Nanotubes: Designed Synthesis, Unusual Reactions, and Coordination Chemistry*, ed. M. A. Petrukhina and L. T. Scott, Wiley, Hoboken, 2012.
18 Y.-T. Wu and J. S. Siegel, *Chem. Rev.*, 2006, **106**, 4843.
19 Y. Shen and C.-F. Chen, *Chem. Rev.*, 2012, **112**, 1463.
20 Y. Segawa, H. Ito and K. Itami, *Nat. Rev. Mater.*, 2016, **1**, 15002.
21 T. Fujikawa, Y. Segawa and K. Itami, *J. Am. Chem. Soc.*, 2015, **137**, 7763.
22 R. Rieger, M. Kastler, V. Enkelmann and K. Müllen, *Chem. – Eur. J.*, 2008, **14**, 6322.
23 S. Hirayama, H. Sakai, Y. Araki, M. Tanaka, M. Imakawa, T. Wada, T. Takenobu and T. Hasobe, *Chem. – Eur. J.*, 2014, **20**, 9081.
24 Y. Yoshida, K. Isomura, Y. Nakamura, H. Kishida and G. Saito, *Chem. Lett.*, 2015, **44**, 709.
25 Y. Yoshida, Y. Nakamura, H. Kishida, H. Hayama, Y. Nakano, H. Yamochi and G. Saito, *CrystEngComm*, 2017, **19**, 3626.
26 E. S. Pysh and N. C. Yang, *J. Am. Chem. Soc.*, 1963, **85**, 2124.
27 J. B. Torrance, J. E. Vazquez, J. J. Mayerle and V. Y. Lee, *Phys. Rev. Lett.*, 1981, **46**, 253.
28 G. Saito and Y. Yoshida, *Bull. Chem. Soc. Jpn.*, 2007, **80**, 1.
29 I. J. Tickle and C. K. Prout, *J. Chem. Soc., Perkin Trans. 2*, 1973, 720.
30 R. M. Williams and S. C. Wallwork, *Acta Crystallogr., Sect. B: Struct. Crystallogr. Cryst. Chem.*, 1968, **24**, 168.
31 C. K. Prout, I. J. Tickle and J. D. Wright, *J. Chem. Soc., Perkin Trans. 2*, 1973, 528.
32 X. Chi, C. Besnard, V. K. Thorsmlle, V. Y. Butko, A. J. Taylor, T. Siegrist and A. P. Ramirez, *Chem. Mater.*, 2004, **16**, 5751.
33 Y. Yoshida *et al.*, unpublished data.
34 T. J. Kistenmacher, T. J. Emge, A. N. Bloch and O. O. Cowan, *Acta Crystallogr., Sect. B: Struct. Crystallogr. Cryst. Chem.*, 1982, **38**, 1193.
35 D. M. Hudgins and L. J. Allamandola, *J. Phys. Chem.*, 1995, **99**, 3033.
36 F. Salama, G. A. Galazutdinov, J. Krełowski, L. J. Allamandola and F. A. Musaev, *Astrophys. J.*, 1999, **526**, 265.
37 A. L. Mattioda, D. M. Hudgins and L. J. Allamandola, *Astrophys. J.*, 2005, **629**, 1188.
38 T. Sugano, Y. Yakushi and H. Kuroda, *Bull. Chem. Soc. Jpn.*, 1978, **51**, 1041.
39 A. Bondi, *J. Phys. Chem.*, 1964, **68**, 441.
40 D. Vermeulen, L. Y. Zhu, K. P. Goetz, P. Hu, H. Jiang, C. S. Day, O. D. Jurchescu, V. Coropceanu, C. Kloc and L. E. McNeil, *J. Phys. Chem. C*, 2014, **118**, 24688.
41 D. Braga, F. Grepioni and E. Tedesco, *Organometallics*, 1998, **17**, 2669.
42 M. Nishio, *CrystEngComm*, 2004, **6**, 130.
43 J. G. White, *J. Chem. Soc.*, 1948, 1398.
44 Crystal data for pristine bper: $C_{22}H_{12}$, M = 276.34, monoclinic space group $P2_1/c$, a = 9.7377(8) Å, b = 11.9539(10) Å, c = 11.3813(10) Å, β = 97.968(1)°, V = 1312.03(19) Å^3, Z = 4, T = 100 K, d_{calc} = 1.399 g cm^{-3}, μ(Mo Kα) = 0.079 mm^{-1}, 2672 reflections used, 199 refined parameters, R_1 = 0.0401 [for $I > 2\sigma(I)$], wR_2 = 0.1267 (all data), GOF = 1.048; CCDC 1537817†.
45 G. R. Desiraju and A. Gavezzotti, *Acta Crystallogr., Sect. B: Struct. Sci.*, 1989, **45**, 473.
46 C. Kröhnke, V. Enkelmann and G. Wegner, *Angew. Chem., Int. Ed. Engl.*, 1980, **19**, 912.
47 V. Enkelmann, K. Göckelmann, G. Wieners and M. Monkenbusch, *Mol. Cryst. Liq. Cryst.*, 1985, **120**, 195.
48 T. Sugano and M. Kinoshita, *Bull. Chem. Soc. Jpn.*, 1989, **62**, 2273.
49 J. B. Torrance, P. S. Bagus, I. Johannsen, A. I. Nazzal, S. S. P. Parkin and P. Batail, *J. Appl. Phys.*, 1988, **63**, 2962.
50 M. Almeida and R. T. Henriques, in *Handbook of Organic Conductive Molecules and Polymers*, ed. H. S. Nalwa, Wiley, 1997, vol. 1, pp. 87–149.
51 G. E. Bacon, *Acta Crystallogr.*, 1951, **4**, 558.
52 (bper)($GaCl_4$), which was recently obtained by the electrochemical oxidation of bper in the presence of (Et_4N)($GaCl_4$) (Fig. S2 in ESI†), involves monocationic bper molecules according to the composition. The length of the bond, which is indicated by an asterisk in the inset of Fig. 8, in (bper)($GaCl_4$) was estimated to be 1.37 Å. Notably, the value is equal to that of charge-rich **bper-4A** in **4**.
53 For several CT complexes, the charge states of electron donor molecules have been estimated on the basis of the bond lengths. For example, see: P. Guionneau, C. J. Kepert, G. Bravic, D. Chasseau, M. R. Truter, M. Kurmoo and P. Day, *Synth. Met.*, 1997, **86**, 1973; G. Fischer and E. Dormann, *Phys. Rev. B: Condens. Matter Mater. Phys.*, 1998, **58**, 7792.
54 Because the charge estimation was performed under the assumption of one orientation of the disordered **bper-4B**, two neighbouring **bper-4A** molecules within the column become nonequivalent. Thus, charges of the two **bper-4A** were estimated to be +0.85 and +0.78 (average charge: +0.82).
55 M. Capone, M. Fabrizio, C. Castellani and E. Tosatti, *Rev. Mod. Phys.*, 2009, **81**, 943 and references therein.
56 M. Che, M. Fournier and J. P. Launay, *J. Chem. Phys.*, 1979, **71**, 1954.
57 M. C. Burla, R. Caliandro, M. Camalli, B. Carrozzini, G. L. Cascarano, L. De Caro, C. Giacovazzo, G. Polidori and R. Spagna, *J. Appl. Crystallogr.*, 2005, **38**, 381.
58 G. M. Sheldrick, *SHELXL-2013*, University of Göttingen, Germany, 2013.
59 K. Raghavachari, *Theor. Chem. Acc.*, 2000, **103**, 361.
60 W. J. Hehre, R. Ditchfield and J. A. Pople, *J. Chem. Phys.*, 1972, **56**, 2257.
61 T. Clark, J. Chandrasekhar, G. W. Spitznagel and P. von Ragué Schleyer, *J. Comput. Chem.*, 1983, **4**, 294.

62 M. J. Frisch, *et al. Gaussian 09, Revision D.01*, Gaussian, Inc., Wallingford, CT, 2009.
63 J. P. Perdew, K. Burke and M. Ernzerhof, *Phys. Rev. Lett.*, 1996, **77**, 3865.
64 P. Giannozzi, *et al.*, *J. Phys.: Condens. Matter*, 2009, **21**, 395502.
65 D. Vanderbilt, *Phys. Rev. B: Condens. Matter Mater. Phys.*, 1990, **41**, 7892.
66 N. Marzari and D. Vanderbilt, *Phys. Rev. B: Condens. Matter Mater. Phys.*, 1997, **56**, 12847.
67 A. A. Mostofi, J. R. Yates, Y.-S. Lee, I. Souza, D. Vanderbilt and N. Marzari, *Comput. Phys. Commun.*, 2008, **178**, 685.

